



# The contributions of atmosphere and ocean to North Atlantic Subtropical Mode Water volume anomalies



Kathryn A. Kelly<sup>a,\*</sup>, Shenfu Dong<sup>b</sup>

<sup>a</sup> Applied Physics Laboratory, Box 355640, University of Washington, Seattle, WA 98195-5640, United States

<sup>b</sup> CIMAS, University of Miami and NOAA AOML, Miami, FL, United States

## ARTICLE INFO

Available online 5 March 2013

### Keywords:

Water masses

Heat loss

Mixing processes

Subduction

Advection

Subtropical Mode Water

## ABSTRACT

Subtropical Mode Water (STMW) in the western North Atlantic Ocean, or Eighteen Degree Water (EDW), as it is commonly known, is formed near the Gulf Stream in the wintertime, is dissipated by mixing and is removed by subduction. The ability of EDW to store and discharge large quantities of heat over periods of several years contributes to the memory of the climate system. To complement the 2-year field and modeling program of the CLIVar MOde Water Dynamics Experiment (CLIMODE) with a perspective of interannual-to-decadal variability (1985–2007), we used a simple box model to hindcast observed EDW volume anomalies in two regions: one in which EDW is formed and an adjacent region of subducted EDW. Estimates of the relative contributions of heat flux anomalies, vertical mixing from Ekman advection, mixing, and circulation are examined using proxy variables derived from winds, sea surface temperature, hydrographic data and altimetric sea level. The importance of each process is evaluated by its contribution to observed EDW volume anomalies in two regions. The study produced some robust conclusions: (1) anomalies of formation by surface heat fluxes are clearly reflected in EDW volume anomalies with some contributions by Ekman advection; (2) of the newly formed EDW about 65% is lost by mixing and about 35% is transferred to the subducted region; (3) mixing losses are well parameterized by the meandering of the nearby GS and (4) transfer and losses from the subducted region can be parameterized by the geostrophic surface flow.

© 2013 Elsevier Ltd. All rights reserved.

## 1. Introduction

The formation of Subtropical Mode Water (STMW) in the western North Atlantic has been attributed to both thermodynamic and dynamic processes (Warren, 1972; Worthington, 1976); its subsequent evolution is the result of mixing, subduction and advection away from the formation region. All of these processes are the subject of a study, the CLIVar MOde Water Dynamics Experiment (CLIMODE), which includes a large field program over a 2-year period as well as related modeling efforts (The CLIMODE Group, 2009).

STMW is formed by wintertime cooling in a region of maximum air–sea heat loss near a western boundary current and is subsequently capped over by warmer waters in the spring. STMW is only exposed to the surface in late fall and winter, so that air–sea interaction occurs within a short time window. STMW formed in one winter can interact with the atmosphere in subsequent winters through entrainment into the mixed layer. STMW is of particular importance in climate processes because it temporally

integrates the ocean's response to heat fluxes, stores heat from one year to the next, and forces turbulent heat fluxes, providing a rare example of ocean feedback in the mid-latitudes (Kelly et al., 2010).

The long renewal time of STMW and its capacity for heat storage make it a leading candidate for observed decadal climate variability in the mid-latitudes. STMW persists beyond the year in which it was formed, owing to the short time window for air–sea interaction, the large volume that interacts with the atmosphere (Warren, 1972) and the tight recirculation that keeps STMW close to its formation site. STMW anomalies can propagate around the subtropical gyre on time scales of 5 years, with properties varying on times scales of 5–10 years (Talley and Raymer, 1982). Estimates of the renewal time of STMW generally ascribe longer times to the North Atlantic, compared with STMW in the North Pacific, with estimates ranging from 2 years to 30 years, increasing with increasing density (Huang and Qiu, 1994; Qiu and Huang, 1995; Suga et al., 2008). Renewal time is important because the longer the renewal time, the longer the memory of the subtropical ocean.

Observed interannual variations in the volume of STMW may be caused by anomalies in formation, in dissipation or in subduction/advection. Analyses of observations from 1993 to 2007 as

\* Corresponding author.

E-mail address: [kkelly@apl.washington.edu](mailto:kkelly@apl.washington.edu) (K.A. Kelly).

part of the Kuroshio Extension System Study (KESS) suggested that mixing dominated in the determination of North Pacific STMW thickness, where the amount of mixing was inferred from the amount of meandering of the KE (Qiu and Chen, 2006; Qiu et al., 2007). Periods when the KE path is “stable” (minimal meandering) are also periods of low eddy kinetic energy; during these “stable” periods the layer of STMW is thick; conversely, the STMW layer is thin when the KE path is unstable. Based on these relationships Qiu and Chen (2006) argue that meandering is a proxy for eddy mixing, which dissipates the STMW. In a comparison of statistics of the Gulf Stream (GS) and the KE derived from sea surface height (SSH), the amount of meandering was further shown to be negatively correlated with current strength, quantified as the SSH difference across the current (Kelly et al., 2010). In contrast with the model of formation by cooling, Qiu and Chen found no clear relationship between North Pacific STMW thickness and surface heat loss anomalies. These results were somewhat contradicted in a modeling study over a 3-year period by Rainville et al. (2007), who attributed interannual variations in STMW formation in large part to heat flux anomalies on short time scales. They also concluded that both advection and mixing are important in the STMW loss in the North Pacific.

In the western North Atlantic the STMW is known as Eighteen Degree Water (EDW), based on its nearly constant temperature. Studies in the North Atlantic highlight a number of processes that may control EDW volume or thickness, including those examined for KESS. There is a robust anti-correlation between EDW thickness and the upper ocean heat content (Kwon, 2003), which is consistent with formation by cooling. Variability of EDW thickness at Bermuda is correlated with the North Atlantic Oscillation and changes in the GS mean path latitude, which may be caused by decadal variations in export of Labrador Sea Water (Joyce et al., 2000). Dong et al. (2007) found that variations in EDW layer thickness are more closely related to changes in advection than to formation and that stratification appears more critical to formation than the strength of the fluxes. Support for the importance of GS meandering in mixing was found in a study by Rajamony et al. (2001) in which the potential vorticity (PV) front was found to move laterally across the GS meanders. Anomalies in EDW volume also may be related to mixed layer depth (MLD): Lagrangian estimates of subduction rates in the GS using Argo float data suggest that a large contribution to subduction is the advection of water out of a deep mixed layer into a region with a shallow mixed layer (Trossman et al., 2009). Ekman effects can contribute both to formation and to subduction. Winds along a front induce cross-front Ekman advection, forcing cold water over the warm current core; the resulting vertical mixing lowers the stratification and increases the outcrop area of cooler waters that leads in turn to increased formation by air–sea fluxes (Thomas, 2005). Rainville et al. (2007) found that while the local effects of down-front winds can exceed those of heat fluxes, the diabatic contributions to formation prevail at larger scales and longer times. Stronger Ekman pumping can also contribute to increased subduction of EDW.

Analyses of the field observations from CLIMODE and modeling studies are steadily improving our understanding of the processes governing EDW anomalies. Analyses of CLIMODE observations (Joyce et al., 2013) suggest that convective processes within the GS are responsible for much of the formation. Restratification by lateral eddy heat fluxes from the GS can contribute to EDW anomalies by decreasing outcrop area (Davis et al., 2013), which in turn decreases the EDW formation rate. In a comparison of the Pacific and Atlantic Maze and Marshall (2013) show that heat flux effects dominate over the frontal/Ekman effects in EDW formation; estimates of EDW formation from climatology by Olsina et al. (2013) are also consistent with this conclusion. Using

assimilation products for 2004–2006 Forget et al. (2011) examined the fate of EDW and found that approximately 2/3 of the EDW was removed by restratification by heat fluxes and 1/3 was dissipated by mixing.

Our study complements other components of CLIMODE in that we examine EDW anomalies on interannual-to-decadal time-scales. The goal of the CLIMODE field program (2004–2006) is to observe and quantify the various processes that contribute to EDW formation and its subsequent evolution. Ocean circulation models assimilating CLIMODE observations create a consistent set of variables with which to reconcile models and observations of EDW processes. We examine more than 20 years of EDW volume estimates and model some of the processes that contribute to them, motivated by CLIMODE observations and previous studies. A box model is used to hindcast the volumes of EDW in two adjacent regions: one in which EDW formation frequently occurs and one in which thick layers of EDW are found, but in which EDW is not formed.

The goal of the box model is to test which of several processes have the greatest impact on interannual EDW volume anomalies, based on a comparison of modeled and observed EDW volumes: formation, mixing, or advection (subduction). Formation anomalies by surface heat fluxes are examined for 1985–2007. Other processes are examined using proxies in the model for a shorter period, 1993–2007. The proxies we examined include down-front winds as a contributor to formation, the GS path length as a contributor to mixing, and geostrophic currents and mixed layer depth (MLD) as contributors to advection (subduction).

In Section 2 we describe the observations of EDW volume, the fields used to calculate formation and the proxies. In Section 3 we examine relationships between the observed variables to motivate the formulation of the model. The model, the various experiments performed, and their evaluation relative to the observations is described in Section 4. Discussion and conclusions are presented in Sections 5 and 6, respectively.

## 2. Data

The domain over which we examined the variables described below is the western North Atlantic 25–45°N and 80–30°W. A subset of this region was used for the model, based on an analysis of EDW statistics, as described in Section 3.1. Data products used in the model are listed in Table 1, along with their sources; examples of the fields of SST, net surface heat flux, and SSH are shown in Fig. 1 to illustrate interannual variability.

An estimate of the formation requires an integral of the net surface heat flux over the outcrop region of a given temperature class. It is desirable to have comparable spatial resolution in the flux fields and in the SST fields used to define the outcrop region, particularly near the GS, where the strong gradients and meandering currents create large anomalies. Great improvements in accuracy and spatial resolution have been made in SST recently, particularly by including all-weather microwave sensors; however, the improved SST fields are only available after 2002. It is also important to have consistent fields over the study period to examine interannual variations in forcing. Based on comparisons of several products<sup>1</sup> with observations from a mooring from CLIMODE (Weller et al., 2013), we selected SST and turbulent fluxes from OAFflux (Yu and Weller, 2007) and radiative fluxes from ISCCP (Schiffer and Rossow, 1983). The ISCCP fields, available daily on a 1° × 1° latitude–longitude grid, are combined with the OAFflux turbulent fluxes to obtain daily maps of net surface

<sup>1</sup> <http://kkelly.apl.washington.edu/projects/climode>

**Table 1**  
Sources of data.

Fields	Source	Web site (http://)
Temperature	NODC	< <a href="http://www.nodc.noaa.gov/OC5/3M_HEAT">www.nodc.noaa.gov/OC5/3M_HEAT</a> >, 3-mo analyzed fields
OISST	NCDC	< <a href="http://www.ncdc.noaa.gov/oa/climate/research/sst/oi-daily.php">www.ncdc.noaa.gov/oa/climate/research/sst/oi-daily.php</a> >
SSH	AVISO <sup>a</sup>	< <a href="http://www.aviso.oceanobs.com/en/data/products/index.html">www.aviso.oceanobs.com/en/data/products/index.html</a> >
Flux, SST	WHOI <sup>b</sup>	< <a href="http://oafux.who.edu">oafux.who.edu</a> >
Wind stress	ECMWF <sup>c</sup>	< <a href="http://rda.ucar.edu/datasets/ds111.1">http://rda.ucar.edu/datasets/ds111.1</a> >

<sup>a</sup> Archiving, Validation and Interpretation of Satellite Oceanographic data.

<sup>b</sup> Funded by the NOAA Climate Observations and Monitoring (COM) program.

<sup>c</sup> TOGA Global Advanced Operational Surface Analysis, distributed by UCAR.

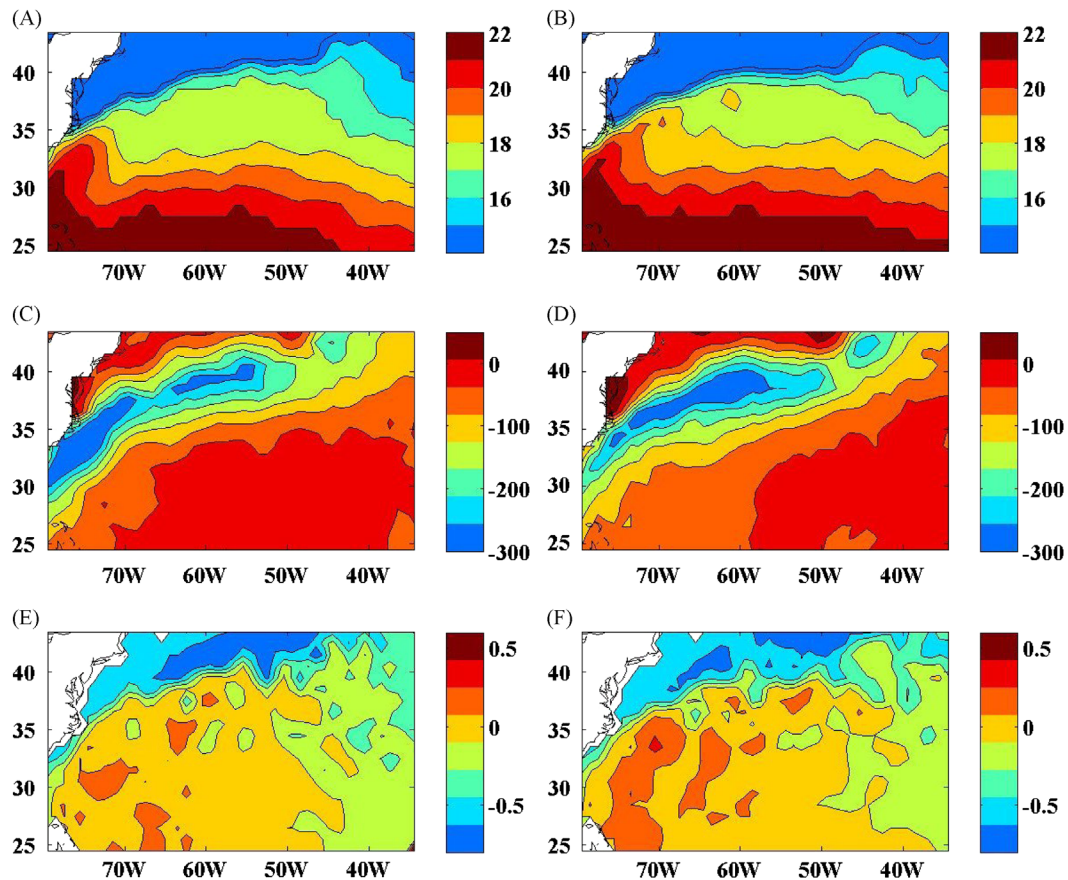


**Fig. 1.** Monthly ocean and flux maps for March 1996 and 2004. (A,B) Sea surface temperature, (C,D) net surface heat flux and (E,F) sea surface height for March 1996 (left column) and March 2004 (right column). (a) SST March 1996, (b) SST March 2004, (c) Qnet March 2004, (d) Qnet March 2004, (e) SSH March 1996 and (f) SSH March 2004.

heat flux  $Q_{net}$  for 1985–2007. Comparisons with fluxes at the mooring (located in a region of high fluxes) showed a  $-37 \text{ W m}^{-2}$  bias (too much cooling) from the net flux product, a relatively small bias compared with other products.

The temperature data used in EDW volume estimates are from the National Oceanographic Data Center (NODC). They are derived from historical hydrographic data, World Ocean Database (WOD) using objective mapping (Levitus et al., 2009). The gridded temperature data are available on a  $1^\circ$  grid with 3-month temporal resolution with seasons defined using the oceanographic convention (JFM, AMJ, JAS, OND). There are a total of 16 vertical levels from the sea surface to a depth of 700 m, with the interval between layers increasing from 10 m at the sea surface to 100 m at depth. The thickness of wintertime (JFM) EDW is shown for each year of the study in Fig. 2. The MLD is also estimated from these temperature maps: here MLD is defined as the depth where the temperature has changed from sea surface temperature by  $0.5^\circ\text{C}$  (Monterey and Levitus, 1997).

The volume of EDW is estimated from temperature profiles at each grid point following two criteria (Kwon, 2003): the temperature must be within the range of  $17\text{--}19^\circ\text{C}$  and the temperature gradient must be no greater than  $0.006^\circ\text{C m}^{-1}$ . We also estimated the volume of water within the range of  $17\text{--}19^\circ\text{C}$  without the gradient constraint; these volumes are approximately twice as large as the volumes with the gradient constraint.

The proxy for Ekman advection includes both wind stress and the mean SST gradient; wind stress is from the European Center for Medium-range Weather Forecasts (ECMWF) TOGA Global Advanced Operational Surface Analysis and the mean SST gradient was derived from NODC's OISST product (Reynolds et al., 2007), which was also used in comparisons with the OAFux SST product.

Proxies for mixing and for loss by advection were obtained from altimetric SSH produced by AVISO (Archiving, Validation and Interpretation of Satellite Oceanographic data); the data are available weekly on a  $1/3^\circ \times 1/3^\circ$  grid (Ducet et al., 2000). The total SSH was derived by combining the anomalous SSH from altimeter and the

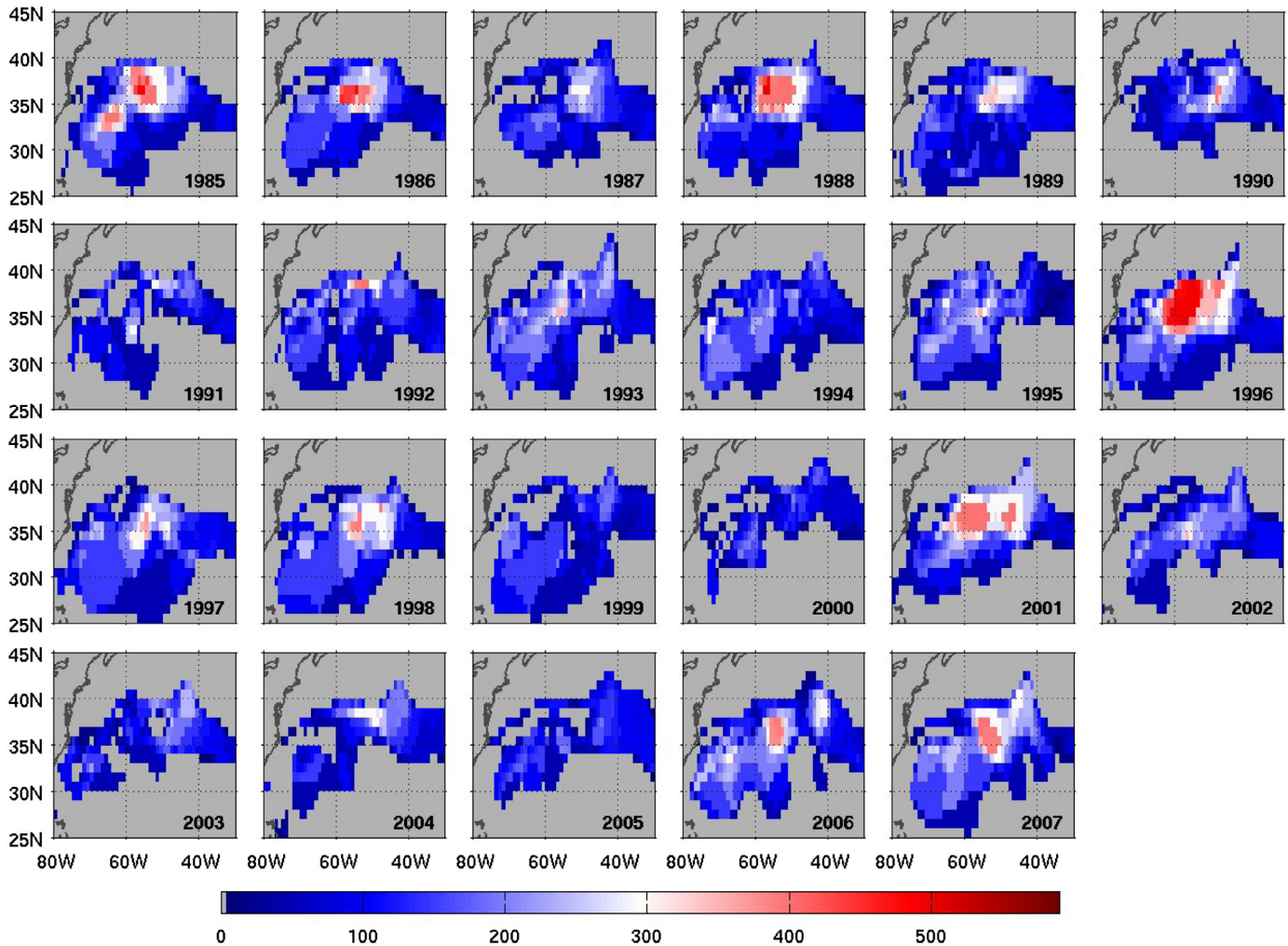


Fig. 2. EDW thickness. Maps of wintertime (JFM) EDW thickness for 1985–2007. Thickness units are meters.

time-mean SSH derived from a combination of GRACE gravity data, SSH and in situ data (Rio and Hernandez, 2004). The GS path was derived from the locations of velocity maxima at each longitude between 75°W and 50°W. No single SSH contour accurately reflects the GS center at all times and locations as in the KE, so an iterative procedure is used. At each time the SSH contour  $h_{GS}$  that corresponds to the maximum geostrophic velocity in the region between 75°W–70°W is estimated. The GS path is then determined by locating velocity maxima along a line perpendicular to  $h_{GS}$  at each longitude. Multiple GS paths may be found at each longitude, reflecting steep GS meanders; locations of velocity maxima are connected to define the actual path. Geostrophic velocity fields were derived from gradients of SSH.

### 3. Analysis of observed and derived variables

The data described above were used to compute estimates of the volume of EDW and of formation by heat fluxes for 1985–2007. The use of proxies derived from altimetric SSH reduces the modeling period to 1993–2007.

#### 3.1. Determination of study regions

The goal in defining the study regions was to find the areas where the processes affecting EDW anomalies can be distinguished statistically. The region of study was defined in terms of statistics of

EDW characteristics; the region simply bounds the area in which the various quantities are computed, but it does not determine their values. For example, formation by heat fluxes is computed by integrating fluxes over the outcrop area for 17–19 °C that is within the region boundaries, not by integrating fluxes over the entire study region. All quantities are summed spatially for the model. Because the study regions are fixed, advection of EDW out of the regions is one of the terms that is included in the model.

To define the model boxes we first found the region where thick EDW is usually found. Using the 23-year WOA data, we tabulated the number of years in which EDW occurs in JFM with a minimum thickness of 100 m (Fig. 3b). Using a minimum thickness corresponding to a nominal MLD eliminates mode water that vanishes seasonally (such as the Madeira Mode Water, Siedler et al., 1987). We used the region that includes the thick EDW about 85% of the time (20 out of 23 years) and made some modifications to obtain a simple, connected region. We then tabulated the number of years in which March SST was between 17 °C and 19 °C (Fig. 3a); the intersection of the region of thick EDW with the region with EDW outcropping in March 85% of the time is statistically a “formation” region (again with slight modifications).

This process defined two distinct spatial regions: (1) where thick EDW usually exists and outcrops in March and (2) where thick EDW exists, but does not usually outcrop (Fig. 3c). We designate these two regions as the “formation” region, where EDW is most likely to be formed, and the “subducted” region

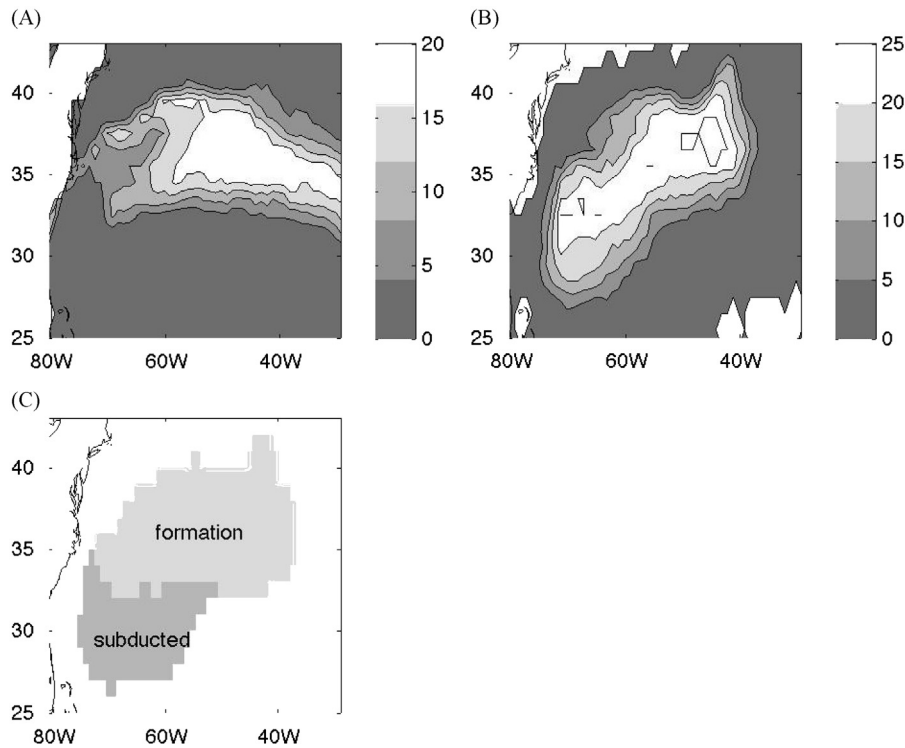


**Fig. 3.** Selection of study region. The number of years in which (A) March SST was between 17 °C and 19 °C and (B) EDW thickness was greater than 100 m in JFM. (C) The two regions defined approximately by statistics in (A) and (B): formation (light gray) and subducted (dark gray). See text for explanation.

where EDW is present, but was probably not formed locally. Subduction may occur in the formation region, that is, the EDW leaves the mixed layer and is not re-entrained the following year. However, it would require a three-dimensional model to determine whether the EDW has been subducted. For our study we will not make this distinction; we will instead model the total EDW volume in each of these two regions. Defining two regions allows us to more easily distinguish the processes responsible for the volume anomalies; formation is neglected in the subducted region, where EDW is assumed to come from the formation region based on the dominant southwestward velocity in both regions.

Changes in EDW volume  $V$  in a Eulerian framework can be written for the formation region as

$$\frac{\partial V_f}{\partial t} = \Delta F - \text{mixing} - \text{transfer} \quad (1)$$

where  $\Delta F$  is the formation of new EDW and the other terms represent loss of volume through mixing and by advection from the formation region to the subducted region. A similar equation can be written for the subducted region volume  $V_s$  as

$$\frac{\partial V_s}{\partial t} = \text{transfer} - \text{loss} \quad (2)$$

where mixing and outflow are combined into a single loss term in the subducted region.

### 3.2. EDW volume in the study regions

EDW volumes were computed for each of the two regions defined above using the WOD and the criteria in Section 2 (Fig. 4a). The combined mean volume for our two regions for winter (autumn) was  $3.9 (2.8) \times 10^{14} \text{ m}^3$ , slightly larger (6–7%) than the corresponding volumes found by Kwon and Riser (2004) using the same criteria. Given the different database, different years and different interpolation methods, we conclude that the

EDW contained within our study regions is the EDW described by Kwon and Riser (2004). These mean volumes are low compared with some historical estimates: the volume of 17–19 °C water estimated by Worthington (1976) was  $16.7 \times 10^{14} \text{ m}^3$ , a factor of 4 larger than our values. The stratification constraint effectively limits EDW to the western basin and, within that basin, reduces the EDW volume by a factor of two. The discrepancy with the Worthington estimate suggests that much of the 17–19 °C volume does not meet the stratification criterion.

The use of a fixed temperature range when the ocean is warming could introduce a bias in our volume time series, regardless of the stratification constraint. We investigated this possibility by returning to the original definition of Mode Water, that is, determining what temperature corresponds to the mode of a histogram by temperature class. The yearly histograms of volume by temperature class for 20–50°N and 80–20°W (Fig. 5) show a trend in temperature mode from about 17.7 °C in 1980 to about 18.2 °C more recently. We compared our volume estimates using a temperature range of 17–19 °C with volume estimates using a range centered on the actual mode, both with the minimum stratification constraint: the differences were small, at most 20% of the mean volume or 1/2 of the standard deviation.

The formation region volumes exhibit a strong seasonal dependence, whereas the subducted region volumes do not. The seasonal cycle of EDW volume is discussed in Section 3.3 in conjunction with the formation estimates. Because heat fluxes have a strong seasonal cycle, this difference is consistent with the statistical partition of the study area into a region in which formation is important and one in which it is not. Time series of EDW volume anomalies in the two regions (Fig. 4b), computed by removing the mean and the annual and semi-annual harmonics, have a high and significant level of correlation,  $\rho = 0.66$ , with a 95% significance level for the correlations of 0.36 (see Appendix for methodology). Hereafter, 95% significance levels will be shown following the correlation as 0.66 [0.36].

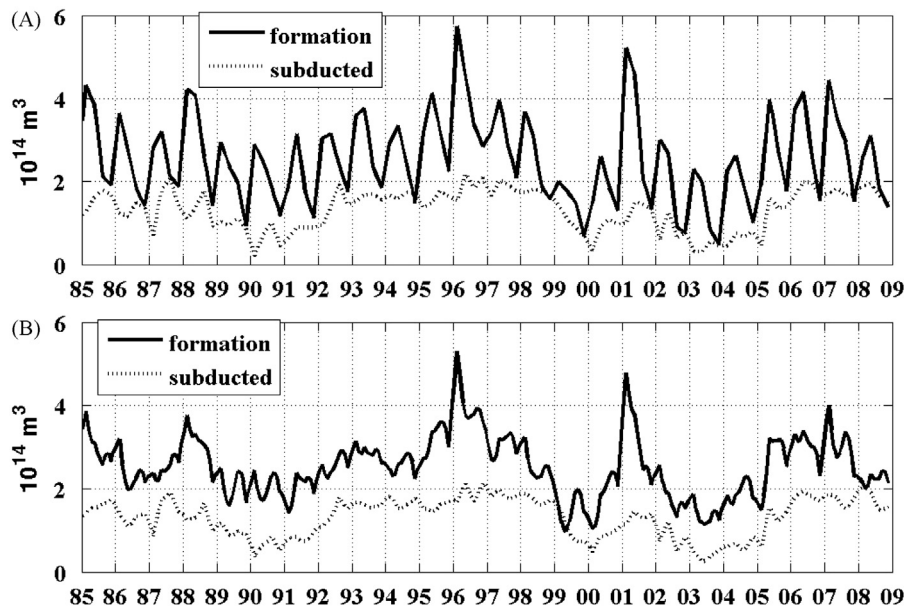


**Fig. 4.** EDW time series in the two regions. (A) Volumes and (B) nonseasonal volumes in formation region (bold) and subtucted region (dotted). EDW was defined as water from 17–19 °C with a vertical temperature gradient of less than  $0.006 \text{ °C m}^{-1}$ . In units of  $10^{14} \text{ m}^3$ .

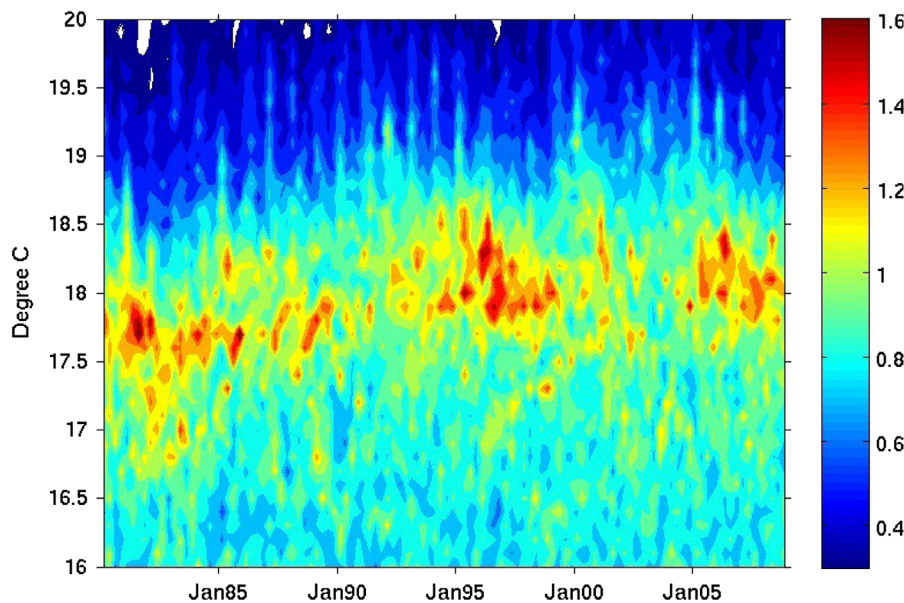


**Fig. 5.** Warming trend in ocean temperature from WOD. Histograms of water volume by temperature class (1980–2008) for 20–50°N and 80–20°W showing temporal variations in the mode of temperature. Units are  $10^{14} \text{ m}^3$  in each  $0.1 \text{ °C}$  bin.

The formation region volume anomalies lead the subtucted region anomalies with a somewhat larger correlation of 0.68 [0.36] by 3 months, the temporal resolution of the observed volumes. The significance of this increased correlation, and therefore whether subtucted region anomalies lag formation region anomalies, depends on the time scales of the anomalies and on the size of the errors. A Monte Carlo simulation was performed using the actual volume anomalies and an estimate of the errors derived from the observations, as described in the Appendix. Based on the null hypothesis of no lag, 95% significance thresholds for the lagged correlation minus the unlagged correlation were generated. A comparison of the increase in correlation with lag from the observations and the significance thresholds shows that there is a significant lag at 6–9 months (Fig. 15a); this suggests movement of EDW from the formation region into the subtucted region, consistent with the

6-month lag noted by Talley and Raymer (1982) between formation and the appearance of EDW at Bermuda (32°N, 64°W) and the lag found by Kwon and Riser (2004). The movement of EDW from the formation region to the subtucted region (with a 2-month lag) was incorporated in the model of EDW in (1) and (2) and in Section 4. Three-month EDW volume anomalies were interpolated to monthly values for consistency with other variables in the model runs.

Other analyses (Dong et al., 2007; Douglass et al., 2011; Kwon, 2003) suggest that an increase in EDW volume corresponds to a decrease in upper ocean heat content and in SSH, a proxy for heat content in this region where temperature variations dominate in density. A comparison of the EDW volumes and SSH shows a similar anti-correlation here (Fig. 6), which is significant in the formation region ( $\rho = -0.53$  [0.35]), but not quite significant in the subtucted region ( $\rho = -0.45$  [0.50]).

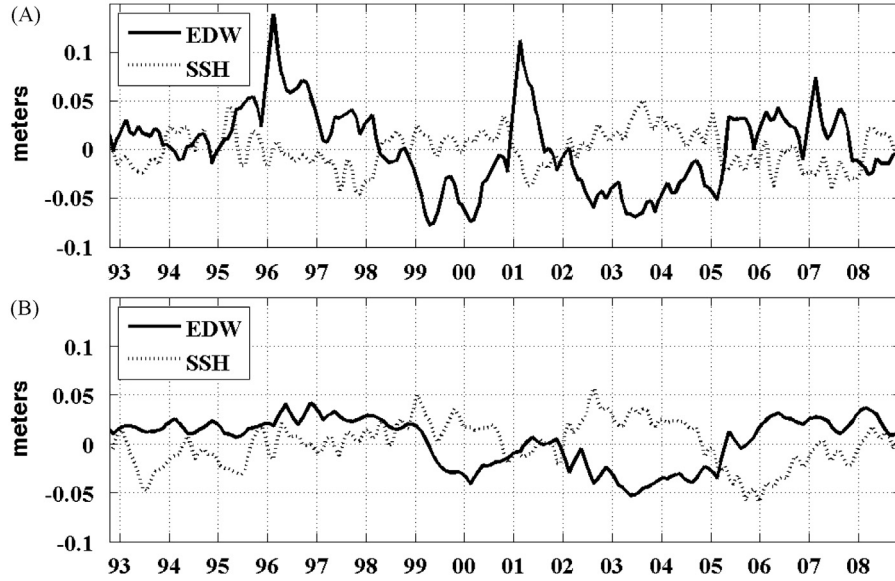


**Fig. 6.** EDW volumes and SSH in the two regions. (A) Volume (bold) and SSH anomalies (dotted) in the (A) formation and (B) subducted regions. SSH is shown in units of meters and volumes from Fig. 4 are scaled for plotting. (A) Formation region anomalies and (B) Subducted region anomalies.

### 3.3. Formation estimates

Our definition of formation was inspired by Walin (1982) as adapted by Maze et al. (2009) and Forget et al. (2011). Formation in the Walin framework is an integration of net surface buoyancy fluxes within known density outcrops that stretch from coast to coast to eliminate the need to estimate advection into and out of the region. The result is an estimate of the amount of water formed within each density class at any location in the ocean. Because the focus of CLIMODE is on EDW, which is confined to the western part of the basin, we modified the Walin formation definition to cover only our study region and included advection as a process in our model. We also neglected freshwater fluxes as in Maze et al. (2009) and Forget et al. (2011), defining outcrops and water classes in terms of temperature.

In the Walin terminology “formation” is the amount of new water formed in a given class by surface fluxes. The “transformation”  $F$  is the rate at which water enters a given class, so that the “formation” rate  $\Delta F$  is derived by subtracting the water leaving a given class from the amount of water entering that class. Transformation  $F$  is defined at each time as

$$F(T_i, t) = \frac{-1}{\rho c_p \Delta T} \sum_i A_i(t) Q_{net}^i(t) \quad (3)$$

where  $Q_{net}^i$  is the net surface heat flux (positive into the ocean) over the outcrop  $A_i$  corresponding to the temperature interval between  $T_i + \Delta T/2$  and  $T_i - \Delta T/2$ .

Formation is then computed as

$$\Delta F(T_i) = F(T_{i+n}) - F(T_{i-n}) \quad (4)$$

where  $n$  depends on the number of outcrops in the temperature class. Although formation can be defined for any temperature class, we will only examine the 17–19 °C class that corresponds to EDW. For 17–19 °C the difference is taken over 2 °C and therefore  $n=2$  for a temperature interval  $\Delta T$  of 0.5 °C. For the model daily formation estimates were averaged to monthly values. The mean JFM formation rate for 17–19 °C is 29 Sv (1 Sv =  $10^6 \text{ m}^3 \text{ s}^{-1}$ ), the difference between the 19 °C transformation rate of 38 Sv and the 17 °C rate of 9 Sv.

A sensitivity analysis using a higher resolution SST field and different values of  $\Delta T$  showed relatively small differences in the wintertime (JFM) or annually averaged EDW formation rates.

Using OISST available on a 0.25° grid (Reynolds et al., 2007) and the OAFflux/ISCCP flux fields on a 1° grid, both re-gridded to 0.5°, gave a mean JFM formation rate that differed from the estimate above by only 1 Sv. Therefore, for consistency with the flux spatial resolution we also used the OAFflux SST fields at 1° resolution. Varying  $\Delta T$  from 0.25 °C to 1.0 °C gave JFM average rates that differed by only 2 Sv and therefore we chose the interval (0.5 °C) used by Maze et al. (2009). Annually averaged formation rates are much smaller than wintertime averages, varying from 4 Sv to about 9 Sv for the 23-year study period.

Monthly estimates of EDW formation show strong seasonal variations. Positive values for both transformation and formation occur in the wintertime; the maximum cooling typically occurs in January, but the maximum transformation to 17–19 °C occurs in February, slightly preceding the maximum outcrop area in March, with monthly magnitudes at times exceeding 50 Sv. Negative values for both terms occur in spring, when fluxes change sign, but taper off as the outcrop shrinks (Speer and Tziperman, 1992). In some studies a distinction is made between “formation” as an increase in EDW volume by wintertime heat fluxes and “destruction” later in the year as a decrease in volume (Forget et al., 2011). However, because our focus is on interannual anomalies we will refer to all heat flux forcing as formation, where a positive formation anomaly indicates a tendency to increase the EDW volume.

To show how formation rate anomalies depend separately on the outcrop area and the flux anomalies, we computed the spatial average of surface heat flux  $\bar{Q}$  over the outcrop  $A_{19}$  in the formation region, as opposed to the sum of the flux over the area as in (3). We illustrate outcrop area contributions to formation using values for 19 °C (Fig. 7), because the 17 °C outcrop area is relatively small. The correlation of wintertime (JFM) monthly EDW formation with  $A_{19}$  is 0.60 [0.24], compared to a correlation of 0.68 [0.24] with heat flux  $\bar{Q}$ ; thus formation depends about equally on flux and on outcrop area anomalies.

A wide range of estimates of EDW volume, formation rate and seasonal cycle in volume that depends on the definition of EDW and on formation has been tabulated from the literature by Forget et al. (2011). Kwon and Riser (2004) estimated the annual volume changes, differencing the late wintertime (FMA) volumes and those of the previous autumn, as  $1.1 \times 10^{14} \text{ m}^3$ . For comparison, the seasonal cycle in our constrained EDW volume estimates (JFM–OND) is  $1.5 \times 10^{14} \text{ m}^3$ . The seasonal cycle for the

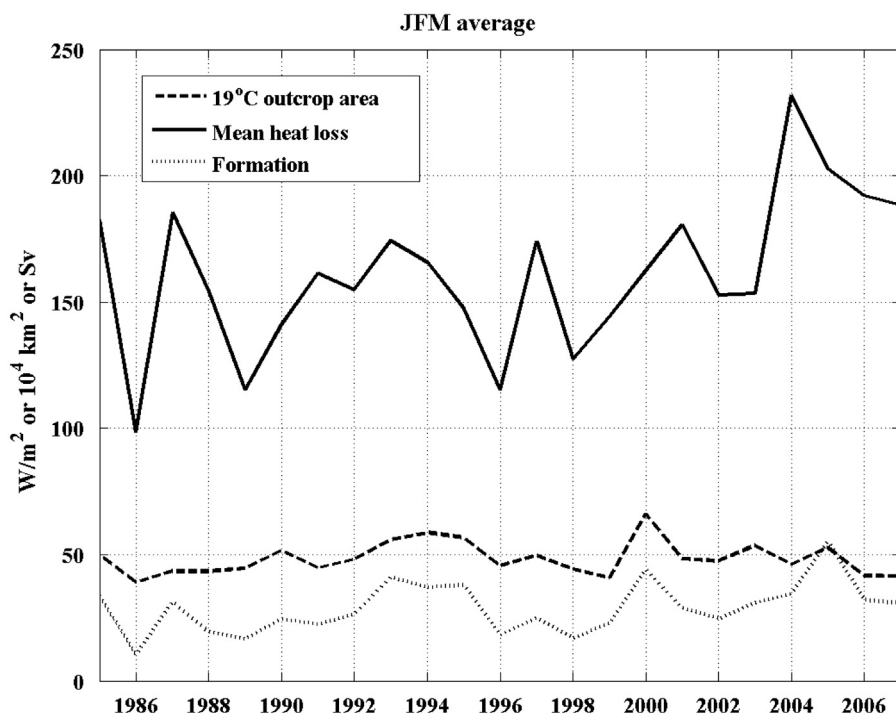


Fig. 7. Wintertime (JFM) outcrop area, heat flux and EDW formation rate. Area of the 19 °C outcrop (dash, units of  $10^4 \text{ km}^2$ ), spatial average of heat loss over this outcrop (solid, units of  $\text{W m}^{-2}$ ), and formation rate for 17–19 °C water (dotted, units of Sv).

unconstrained volumes is smaller than that for the constrained volumes, so that the addition of the stratification criterion does not reduce the seasonal cycle of volume.

The seasonal cycle of formation should be consistent with the observed seasonal cycle of EDW volume. In the formation region we estimate formation as  $2.4 \times 10^{14} \text{ m}^3$ , which combined with the unconstrained volume ( $8.4 \times 10^{14} \text{ m}^3$ ) gives a 29% annual renewal rate. The JFM formation from heat fluxes is  $2.8 \times 10^{14} \text{ m}^3$ , substantially larger than the annual mean. One explanation for the large seasonal cycle of heat flux formation relative to that of the observed EDW volume is the poor temporal resolution in the volume estimates. Volumes from monthly Argo data (2004–2010) have a maximum in April, a poor match with the JFM mean, and a seasonal difference of about  $2.7 \times 10^{14} \text{ m}^3$ , nearly the same as the JFM formation by heat fluxes.

Formation rates clearly depend on the flux product, a topic that has been explored by Forget et al. (2011). To illustrate the effect on our analysis of a simple bias in fluxes, we added  $20 \text{ W m}^{-2}$  to the net flux everywhere in the region, assuming that the  $-37 \text{ W m}^{-2}$  bias in the GS (Section 2) is indicative of bias sign, but is larger than average. The adjusted JFM formation rate dropped to  $2.0 \times 10^{14} \text{ m}^3$ , less than the Argo-based seasonal volume difference. Because mixing and subduction of EDW occur all year, formation should exceed the observed wintertime volume increase by the amount of wintertime loss. This suggests either that the fluxes do not have an appreciable bias or that there are other sources of formation.

The difficulty in reconciling mean volume budgets led us to formulate models to reproduce volume anomalies; the models in Section 4 are insensitive to the mean formation rate.

### 3.4. Factors affecting EDW formation

EDW can be formed by thermodynamical or dynamical processes. Because formation by surface heat fluxes is defined in terms of observed outcrop area and a flux product derived from

observations, several important factors in formation by heat flux forcing are implicit and cannot be modeled here. These factors include advection, which can change the outcrop area, feedback effects of the ocean heat content on fluxes, as well as the many factors that influence fluxes, such as changes in wind speed.

An analysis of the seasonal cycle of SST and surface heat flux  $Q_{net}$  suggests a strong influence of the nearby Gulf Stream on restratification, with consequences for outcrop area and formation (Fig. 8). Using a representative region where the mean GS path is nearly zonal (60–50°W), both variables were averaged over this longitude range in 2° latitude bins. Temperature tendency  $\partial T/\partial t$  in this region has virtually no dependence on latitude (Fig. 8a), with ocean warming beginning on about day 75 of any year. However, the onset of surface heating (the zero-crossing of  $Q_{net}$ ) has a strong latitudinal dependence, with ocean warming  $\partial T/\partial t$  leading the onset of surface heating by an amount that increases with latitude (increasing proximity to the GS) (Fig. 8b). Ocean warming precedes the onset of surface heating by about 1 week at 32–34°N, increasing to nearly 2 months in the GS (38–40°N). An analysis and model of the temperatures at two CLIMODE moorings suggests that the warm advection is from eddy heat fluxes (Davis et al., 2013). Clearly a local balance between surface heating and ocean warming only exists away from the GS. More GS warm advection results in a warmer ocean, a smaller 17–19 °C outcrop and, for a fixed value of the surface heat flux, a smaller formation term for 17–19 °C.

The increase in ocean heat content (and SSH) associated with reduced EDW volume (Fig. 6) has a feedback effect on the air–sea heat fluxes: an increase in heat content corresponds to an increase in SST and therefore an increase in heat loss to the atmosphere. An examination of monthly SSH (as a proxy for heat content) and net surface heat flux anomalies in the formation region shows a significant anti-correlation ( $\rho = -0.35$  [0.25], Fig. 15b), with SSH anomalies leading flux anomalies by 2 months (see Appendix for details, cf. Kelly et al., 2010). The magnitude of this feedback is about 10% of the flux anomaly. The

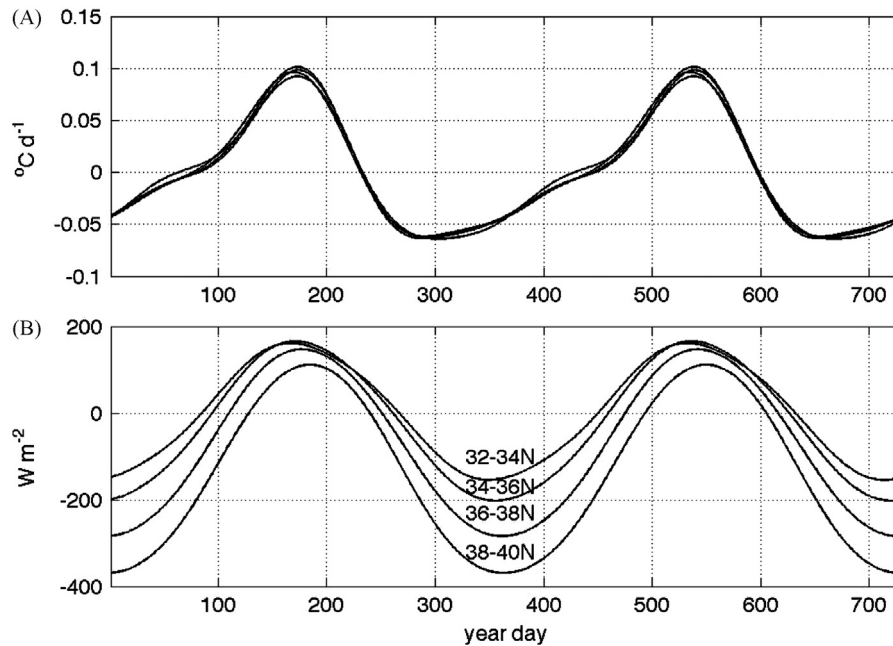


**Fig. 8.** Annual cycle of ocean temperature tendency and surface fluxes. (A) Temperature tendency in units of  $^{\circ}\text{C d}^{-1}$  and (B) net surface heat flux in units of  $\text{W m}^{-2}$ , averaged over  $60\text{--}50^{\circ}\text{W}$  in  $2^{\circ}$  latitude bins from  $32\text{--}34^{\circ}\text{N}$  to  $38\text{--}40^{\circ}\text{N}$ . The onset of ocean warming (zero crossing in (A)) occurs at nearly the same time regardless of proximity to the Gulf Stream ( $38\text{--}40^{\circ}\text{N}$ ), while the onset of surface heating (zero crossing in (B)) occurs up to 2 months later.

anticorrelation of SSH and EDW volume suggests that more EDW (lower heat content) should decrease formation by decreasing the heat loss (negative feedback); however, it is also possible that more EDW will increase the outcrop area for  $17\text{--}19^{\circ}\text{C}$ , a positive feedback. These two competing effects cannot be adequately separated using the observed fields and are implicit in the formation term.

Wind stress directed down the GS front produces an Ekman advection across the temperature gradient (Joyce et al., 2013) that can affect EDW volume in two ways: (1) an increase in the  $17\text{--}19^{\circ}\text{C}$  outcrop area and (2) vertical mixing that decreases the stratification. The impact on outcrop area is implicit in the heat flux forcing; however, the second effect is not. A simple proxy for Ekman advection is derived from

$$A_{Ek}(t) = -\hat{k} \times \vec{\tau}(t) \cdot \nabla T_{MLD} \quad (5)$$

where  $\vec{\tau}$  is the time-varying wind stress,  $\hat{k}$  is a unit vector in the vertical and  $\nabla T_{MLD}$  is the mixed layer temperature gradient. Here we approximate the  $\nabla T_{MLD}$  with the mean SST gradient and spatially average (5) over the formation region. The mean and standard deviation of this proxy ( $1.7 \times 10^{-4}$  and  $1.5 \times 10^{-4} \text{ N m}^{-3} \text{ }^{\circ}\text{C}$ , respectively) are used to obtain a normalized version  $\hat{A}_{Ek}$  of the proxy (Fig. 10a, thin line); the standard deviation is nearly 90% of the mean value.

### 3.5. Factors affecting EDW transfer and loss

Contributors to EDW loss are mixing and in this Eulerian analysis advection out of the region. The effects of these terms were parameterized using proxies.

Following Qiu and Chen (2006) we used the path length derived from altimetric SSH (Figs. 9 and 10b, thin line) as a mixing proxy; the method for characterizing the GS path length differs slightly from their method and is described briefly in Section 2. The mean path length was about 3400 km, with a standard deviation of about 350 km, about 10% of the mean.

Based on the study by Trossman et al. (2009) we reasoned that transfer of EDW from the formation region with its deep mixed

layer to the subtended region with a warmer shallow mixed layer could be proportional to the difference in MLD between the two regions. The spatially averaged difference in MLD between the formation and the subtended regions was a proxy for this contribution (Fig. 10a, thick line). The mean MLD difference was 20 m with a comparable magnitude for standard deviation of 21 m.

Following Dong et al. (2007) we used spatially averaged southward geostrophic velocity as a proxy in our model for advection of EDW (Fig. 10b, thick line). Advection out of the formation region and into the subtended region was denoted as “transfer,” as in (1) and (2); advection out of the subtended region was designated as “loss.” In the spatial average we exclude the region with large velocities near the GS. The meridional velocity in both regions is predominantly southwestward, consistent with a transfer of EDW from the formation region to the subtended region. Based on the mean velocity of  $-0.010 \text{ m s}^{-1}$ , the distance over which the EDW would be advected in the 6–9 month lag between the volume time series (Fig. 15a) is about 160–240 km, less than the approximately 600 km separating the centers of the two regions. A gradual decrease in EDW volume as it is advected southward would give greater weight to EDW near the boundary than to EDW elsewhere in the region, so that the 6–9 month lag may represent the advective time scale weighted by the volume anomaly. The standard deviation of velocity was  $0.0038 \text{ m s}^{-1}$ , more than 30% of the mean value.

## 4. Model for EDW volume changes

The volumes in the formation and subtended regions are modeled using versions of Eqs. (1) and (2), respectively. The models were initialized with observed volumes and were integrated forward with a monthly time step. The two regions are linked in the model in that the outflow of the formation region is the inflow to the subtended region (“transfer”). We began with the simplest model and increased the complexity by adding processes by proxy, comparing hindcasts of volumes in each

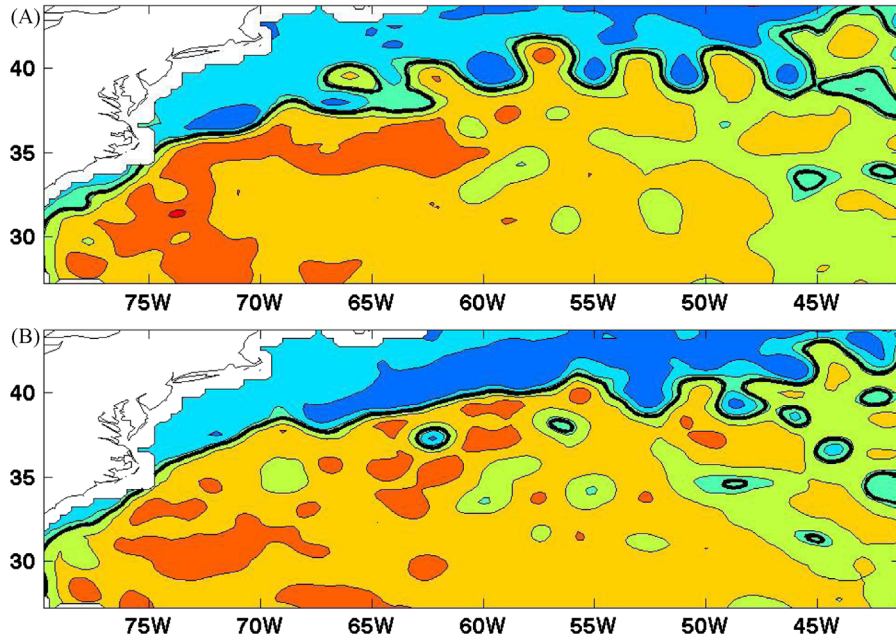


Fig. 9. Path length from altimetric SSH. Maps showing Gulf Stream path used for mixing proxy for (a) March 1993 and (b) March 1996.

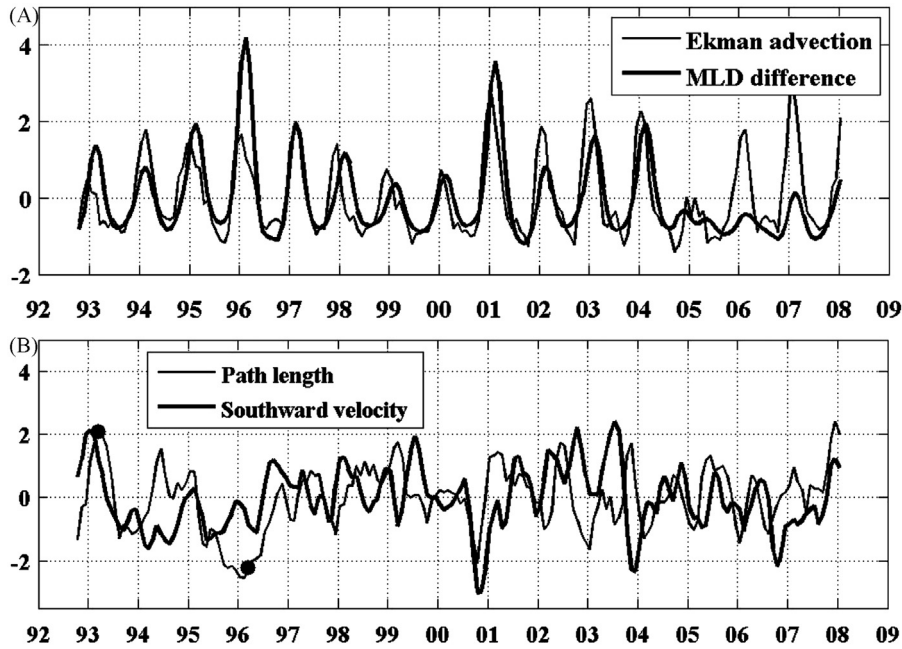


Fig. 10. Normalized proxies for EDW model. (A) Ekman advection (thin line) and MLD in formation region minus MLD in subducted region (thick line) and (B) path length of the Gulf Stream (thin line) and southward geostrophic velocity (thick line). Dots in (B) correspond to path length values for the paths shown in Fig. 9. Proxies were normalized by their standard deviation and the mean was removed.

region to the observed volumes. The metric for the ability of the model to reproduce the observed volume  $V_{obs}$  is the “skill,” or the fraction of volume variance  $\sigma^2(V_{obs})$  described by the model  $V_{mod}$ , given in terms of the model error by

$$S = 1 - \frac{\langle [V_{mod} - V_{obs}]^2 \rangle}{\sigma^2(V_{obs})} \quad (6)$$

where  $\langle \cdot \rangle$  is an average over the monthly volume estimates and the skill is computed separately for each of the two regions.

In all eight models examined: two were without proxies and six were with proxies. The first two models were run and compared for the entire 23 years and then Model 2 and the latter

six were run for 15 years beginning with 1993. The comparisons of skill for Models 2–8 in Table 2 were based on the 15-year common period.

#### 4.1. Models without proxies

The simplest model (Model 1) is the response of the formation region volume to the heat flux formation  $\Delta F$  defined in (3) and (4)

$$V_f(t + \delta t) = V_f(t) + \delta t[\Delta F(t) - \langle \Delta F \rangle] \quad (7)$$

Mixing and transfer have been combined here into a single constant loss term that balances the mean formation rate, so that there is no

trend in EDW volume, consistent with the observed volumes. The lack of time dependence in the loss term  $\langle \Delta F \rangle$  renders the subducted region model trivial and therefore Model 1 cannot distinguish between transfer and loss in the formation region.

Model 1 reproduces well the seasonal cycle of volume (Fig. 11), as well as reproducing some of the observed EDW anomalies. Agreement with the seasonal cycle of observed volumes suggests that heat flux forcing is responsible for the seasonal cycle of volume anomalies, although the WOD values may be an underestimate, as suggested by Argo comparisons. This formation-only model accounts for 14% (24%) of the observed volume variations in the formation region for 1985–2007 (1993–2007). Although much of that skill arises from the seasonal cycle, modeled volume anomalies in Fig. 11 clearly reproduce some of the observed decadal-scale anomalies.

Temporally varying EDW volume in the subducted region must be induced by temporal variations in the transfer rate, for which a likely contributor is the magnitude of EDW volume anomalies in the formation region: for years in which more EDW is formed, more

EDW will be transferred to the subducted region. A similar argument can be made for mixing or loss, that the rate of decrease of volume should be proportional to the current EDW volume, as

$$\frac{\partial V}{\partial t} = -cV(t) \tag{8}$$

where  $c$  is a constant. A comparison of the reduction of EDW volume in the formation region from spring to fall (OND minus AMJ) with wintertime (JFM) EDW volume from the WOD reveals a marginally significant negative correlation ( $\rho = -0.37$  [0.37], Fig. 12). EDW reduction in the subducted region is not significantly anticorrelated with JFM volume  $V_s$ ; however, unconstrained EDW reduction is significantly anticorrelated with JFM volume in both regions. Loss rates may actually be proportional to variables other than volume, such as the thickness of the EDW or the size of the surface area in contact with other water masses; however, these variables are likely to be correlated with volume and their addition here would require a more complex model.

This relationship (8) motivated a parameterization of EDW mixing, transfer and loss in terms of current volumes for all subsequent models. With the addition of proportional mixing and proportional transfer, the formation region volume  $V_f$  is modeled as

$$V_f(t + \delta t) = V_f(t) + \delta t[\Delta F(t) - \alpha C_f V_f(t) - \beta C_f V_f(t)] \tag{9}$$

where  $C_f = \langle \Delta F \rangle / \langle V_f \rangle$  is a scaling factor and  $\alpha$  and  $\beta$  are the coefficients of the mixing and transfer terms, respectively, with mean values between 0 and 1. With transfer and losses proportional to EDW volume, the subducted region volume  $V_s$  was modeled as

$$V_s(t + \delta t) = V_s(t) + \delta t[\beta C_f V_f(t) - \gamma C_s V_s(t)] \tag{10}$$

where  $C_s = \langle \Delta F \rangle / \langle V_s \rangle$ , and  $\gamma$  is the coefficient of the loss term. In all subsequent models mixing, transfer and loss are proportional to

**Table 2**  
Skill of models for 1993–2007.

No.	Formation	Subducted	Description/proxies
1	0.24	N/A	Constant loss rate
2	0.39	0.32	Volume proportional, constant coefficients
3	0.43	0.31	Formation includes Ekman advection
4	0.58	0.50	Path-length mixing
5	0.55	0.36	Path-length plus MLD transfer
6	0.64	0.02	Path-length plus $-v_g$ transfer
7	0.58	0.66	Path-length plus $-v_g$ loss
8	0.64	0.53	Path-length plus $-v_g$ transfer and loss

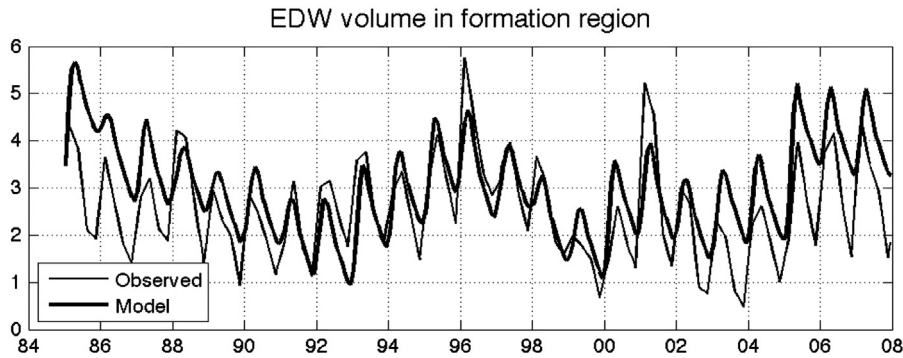


**Fig. 11.** Model using actual formation with a constant loss rate. Model 1 of EDW volume (thick line) in the formation region and observed volumes (thin line). Units are  $10^{14} \text{ m}^3$ .

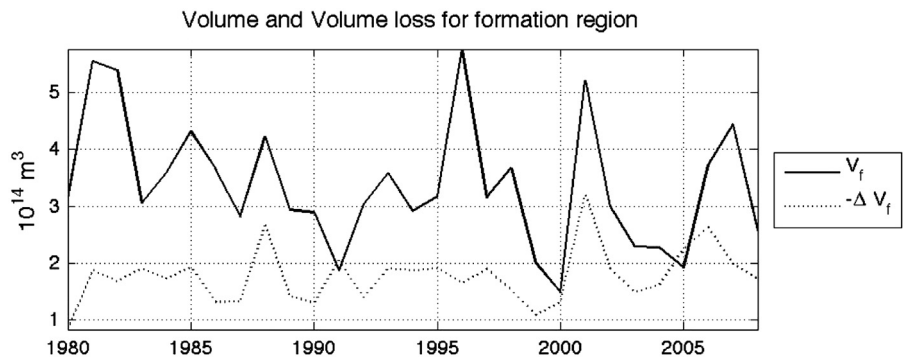


**Fig. 12.** Proportionality of EDW loss and EDW wintertime volumes. Loss of EDW (dashed line) from spring to fall (OND minus AMJ) and wintertime (JFM) EDW volume (solid) from WOD. The negative correlation between EDW loss rate and wintertime volume suggests a parameterization of loss rate based on volume.

volume as in (9) and (10) above, while the coefficients vary. The relative sizes of  $\alpha$  and  $\beta$  determine what fraction of 17–19 °C water is transferred to the subducted region as EDW. The coefficient  $\gamma$  determines what fraction is lost from the subducted region. The lack of an observed trend in the EDW volumes in either region requires that  $\langle\alpha\rangle + \langle\beta\rangle \approx 1$  and that  $\langle\beta\rangle \approx \langle\gamma\rangle$ . Note that the model is insensitive to the mean formation rate as all the terms scale with this factor.

Model 2 combines heat flux forcing with proportional mixing, transfer and loss (9) and (10) using constant coefficients  $\alpha_0$ ,  $\beta_0$ , and  $\gamma_0$ . The values of the coefficients that gave the highest skill  $S$  were  $\alpha_0 = 0.65$ ,  $\beta_0 = 0.35$  and  $\gamma_0 = 0.35$  so that the transfer rate is approximately 35% of the formation rate. The remaining 65% of the new volume from heat flux forcing dissipates over the year, presumably by mixing. For the 23-year period, Model 2 had skills of 39% and 21%, respectively, for the formation and subducted regions; these values differ somewhat from those shown in Table 2, for which skill was computed only over the 15-year common period for the proxies. Proportional mixing clearly increases the skill of the formation-only Model 1 and describes some of the volume variations in the subducted region. Making the terms proportional to volume significantly improves the model and therefore this formulation was retained for all subsequent models.

#### 4.2. Models with proxies

The next set of models incorporated proxies for some of the terms and the skill for each model was calculated based on their common period (1993–2007). The purpose of including the proxies was to diagnose which processes contribute most to the temporal changes in EDW volume based on the skill of the models (see Appendix for the methodology for evaluating the significance of an improvement in skill by adding parameters).

Three of the four proxies are modifications for the transfer or loss rate of EDW; the Ekman proxy  $A_{Ek}$  is different in that it supplements, rather than modifies, formation. The effect of Ekman advection on outcrop area is implicit in the definition of heat flux formation  $\Delta F$ , as discussed above; therefore, the intent of this proxy is to test for an additional contribution of Ekman advection to formation.

Normalized proxies were used to test relative contributions from various terms. Each proxy was first normalized to have a mean of zero and a standard deviation of one. The Ekman proxy was added to the heat flux forcing to create a formation term

$$\Delta F + \delta_0 \langle \Delta F \rangle \tilde{A}_{Ek} \quad (11)$$

where  $0 < \delta_0 < 1$ . The other normalized proxies were scaled with an amplitude factor of 0.5 and incorporated into a volume-proportional term. For example, for a modification of mixing by GS path length

$$\alpha(t) = \alpha_0 [1 + 0.5 \tilde{L}(t)] \quad (12)$$

where  $\tilde{L}$  is the path length anomaly normalized by its standard deviation. The one is added to insure that the term is generally positive, as the sign of the proxy is determined by its representation of a given physical process. The previous values for  $\alpha_0$ ,  $\beta_0$  and  $\gamma_0$  were retained in all of the models; this formulation (12) leaves the mean value of the term unchanged, that is,  $\langle\alpha(t)\rangle = \alpha_0$ . The proxy for geostrophic advection is  $-v_g$  as a larger southward velocity corresponds to more transfer between regions and more loss out of the subducted region. Each of these proxies (Ekman advection  $A_{Ek}$ , path length  $L$ , MLD difference  $\Delta h$  and southward velocity  $-v_g$ ) was in turn incorporated into a model of EDW volume anomalies.

Model 3 is the same as Model 2 except that formation solely by heat fluxes is replaced with the modified formation (11). This model has the only adjustable parameter  $\delta_0$  in the proxy models. Estimates of the relative contributions of Ekman advection and heat-flux forcing to formation vary widely (Joyce et al., 2013); therefore, a range of values for  $\delta_0$  was tested. The maximum skill for Model 3 was for  $\delta_0 = 0.3$ , a small, but significant increase of skill over that of Model 2 (Table 2). Owing to the small change in skill, heat flux forcing only was used in subsequent models.

Model 4 tested whether path instabilities parameterize time-varying mixing; we incorporated the GS path length into the mixing coefficient  $\alpha$  as in (12) above. This change substantially improved the skill of the model for both regions to 58% and 50%, respectively (Table 2 and Fig. 13). This proxy so clearly improved the fit to observed volumes that it was retained for Models 5–8.

Model 5 tested whether differences in MLD between the two regions parameterize the transfer of EDW from the formation region to the subducted region. If the transfer of EDW represents actual subduction of water out of the mixed layer, then the time-varying difference in MLDs between the two regions should be important; the addition of normalized MLD difference  $\Delta h(t)$  to the transfer coefficient as  $\beta(t) = \beta_0(1 + 0.5\Delta h)$ , as in (12), did not improve the model skill (Table 2). The skill dropped slightly in the formation region (to 55%) and substantially in the subducted region (to 36%). This proxy was not used in subsequent models.

Geostrophic velocity  $-v_g$  was tested for the transfer term, the loss term, or for both terms. Model 6 tested whether changes in the meridional velocity parameterize the transfer of EDW. The proxy  $-v_g$  was incorporated into  $\beta$ , analogous to how  $\Delta h$  was included in Model 5. This proxy improved the formation region skill, but greatly decreased the subducted region skill. Model 7 tested the proxy  $-v_g$  in the loss coefficient ( $\gamma$ ): this modification to the loss term substantially improved the skill in the subducted region from 50% for Model 4 to 66% (the formation region is not affected by this term). Finally, the proxy  $-v_g$  was included in both transfer and loss in Model 8: the skill for the subducted region dropped to 53% and the skill in the formation region is identical to that for Model 6 (Table 2).

## 5. Discussion

A simple model was developed to hindcast the volumes of EDW in two adjacent regions: one in which EDW formation frequently occurs and one in which thick layers of EDW are found but in which EDW does not outcrop. Several versions of the model showed good skill in reproducing volume anomalies in both regions.

The goal of the model was to test several processes that contribute to EDW formation and loss to determine which have the greatest effect by comparing modeled and observed EDW volumes. In the formation region, the processes included formation, mixing and transfer of EDW to the subducted region by advection. In the subducted region the factors included inflow of EDW from the formation region and loss of EDW; unlike in the formation region, this loss is not divided into mixing and advection. Formation by heat fluxes (computed from observed fields) forced all of the models; the effect of processes other than formation by heat fluxes was tested using proxy variables. The proxies derived from altimetric SSH, GS path length for mixing and geostrophic velocity for advection, were only available starting in 1993; therefore, the models using proxies were run and compared using the shorter period, 1993–2007 (Table 2).

Although we used a statistical test designed for a linear regression for evaluation of the models, as described in the Appendix, the models contain fewer free parameters than

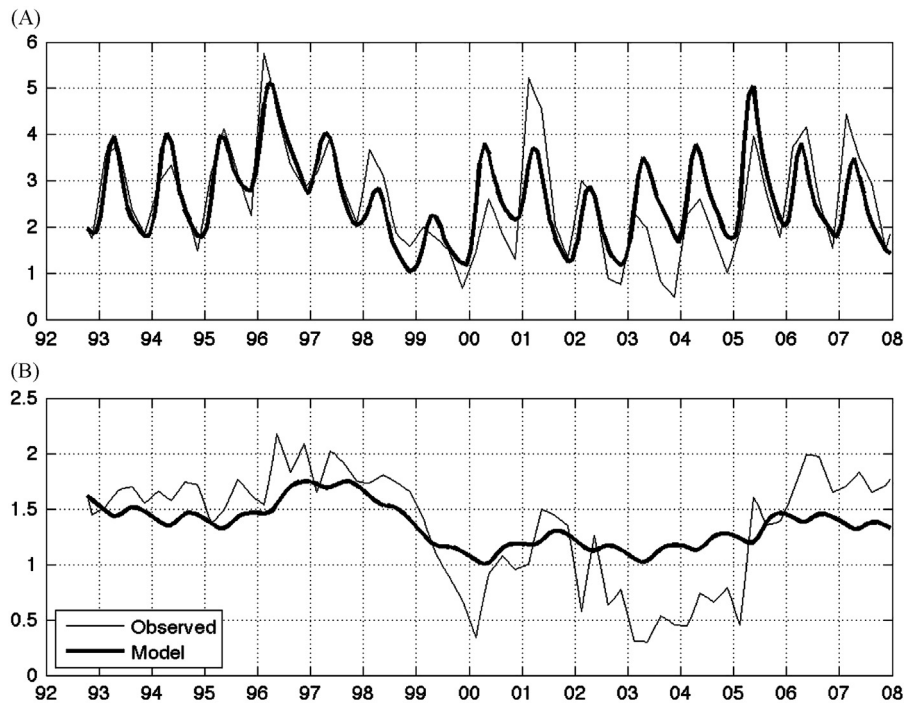


**Fig. 13.** Model using path length proxy for mixing. Model 4 of EDW volume (thick line) in the (A) formation and (B) subtended region and observed volumes (thin line). Units are  $10^{14} \text{ m}^3$ .

processes, unlike a linear regression. Except for the Ekman proxy (11), the normalized proxies are each inserted into the model with the same constant coefficients ( $\alpha_0$ ,  $\beta_0$ , and  $\gamma_0$ ) to constrain their mean values. These constraints make the model skill test more stringent than is needed to evaluate the contributions of the various processes.

The explicit heat flux formation  $\Delta F$  in the model was derived from net surface heat fluxes summed over the outcrops for  $17^\circ\text{C}$  and  $19^\circ\text{C}$ , the nominal temperature limits for EDW. The advantage of this calculation is its accuracy; the disadvantage is that the contributions to  $\Delta F$  are not modeled. Because of the proximity of the EDW to the Gulf Stream, it is likely that both geostrophic and Ekman advection play a role in EDW formation (Fig. 8 and Joyce et al., 2013). Both of these variables likely have the signature of the North Atlantic Oscillation (NAO, Joyce et al., 2000); in addition, there are several variables with a NAO signature (winds, air temperature, humidity) that create flux anomalies (see, for example, articles in Hurrell et al., 2003). These effects are implicit in this model.

The effect of formation anomalies alone on observed EDW volumes was examined in Model 1 by keeping the loss of EDW at a constant value (Fig. 11). The formation estimates reproduce well the seasonal cycle of EDW volumes in the formation region and account for 24% of the EDW volume variance (Table 2). This significant skill level suggests that heat fluxes account for most of the seasonal cycle of EDW volume and that the heat flux anomalies make a significant contribution to anomalies in EDW volume. A heat flux bias was shown in Section 3.3 to alter the amplitude of the seasonal cycle of formation; the good agreement in observed and modeled seasonal volumes suggests that the OAFIux/ISCCP heat flux biases are small. In all of the models the transfer and loss terms are scaled by the mean annual formation rate  $\langle \Delta F \rangle$ , which makes the model relatively insensitive to this mean rate.

Observations of loss relative to volume (Fig. 12) motivated the formulation of transfer and loss in terms of current EDW volumes. The volume-proportional transfer in Model 2 adds some simple

physics to the model: it propagates EDW volume anomalies into the subtended region, which is consistent with the observation that the volume anomalies in the two regions are lag-correlated (Fig. 4b). If the volume proportional formulation is not considered the addition of another process, then heat flux forcing alone accounts for 39% of the formation region volume variance. The volume proportional formulation was retained in all subsequent models.

For consistency with other CLIMODE studies we imposed a maximum stratification constraint (in addition to the temperature class) in the definition of EDW volume observations. The addition of the constraint reduced observed volume estimates by a factor of two. The requirement to match modeled volumes to the smaller constrained EDW volumes requires careful interpretation of the terms in the formation region model. Heat flux forcing gives an estimate of the  $17\text{--}19^\circ\text{C}$  volume, without reference to stratification. The best-fit constant coefficient  $\alpha_0$  in (9) and (10) gives a transfer rate of EDW from the formation region to the subtended region of 35% of the formation rate; this can be interpreted as the success rate of subduction: that is, about 1/3 of newly formed  $17\text{--}19^\circ\text{C}$  water arrives at the subtended region within the specified stratification.

What is the correct interpretation of the fate of the remaining 65% of formation by heat fluxes? The success of the path length proxy in describing anomalies around the mean loss rate suggests that mixing is a large contributor to the loss. Based on the factor of two discrepancy between constrained and unconstrained volumes, much of the newly formed  $17\text{--}19^\circ\text{C}$  water does not meet the stratification criterion and therefore contributes to this loss term in the model; some of that water may have been transferred to the subduction region but is not included in the observed or modeled volumes there. The seasonal loss of EDW by restratification by heat fluxes is included in the heat flux forcing, so it does not contribute to this loss.

The effects of Ekman advection on outcrop area are implicit in the formation term  $\Delta F$ , which is derived from observations. To determine whether there is any additional effect of down-front winds on

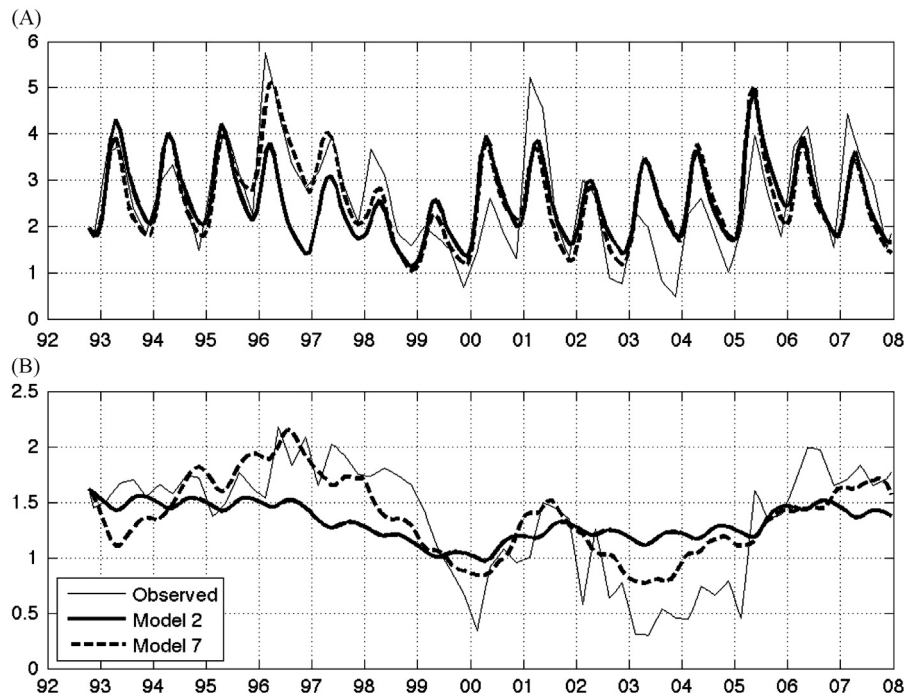


**Fig. 14.** Comparison of models with and without proxies. Model 2 with proportional mixing, transfer and loss (thick solid line). Model 7 with addition of path length mixing and incorporating the geostrophic velocity proxy (thick dashed line) compared with observations (thin line). See model descriptions in Table 2. Units are  $10^{14} \text{ m}^3$ . (A) EDW volume in Formation region and (B) EDW volume in Subducted region.

formation, we incorporated the Ekman advection proxy (5) as an additional formation term (11). The best fit for the Ekman proxy formation was about 18% as large as the heat flux formation anomalies; the increase in skill was small, but significant (Table 2). This result suggests that the decrease in stratification associated with advecting cold water over warm water may make a contribution to EDW volume beyond that of its effect on outcrop area.

The addition of mixing, parameterized in terms of the GS path length as in Qiu and Chen (2006), increased the skill of Model 4 from 39% to 58% of the volume variance in the formation region, relative to Model 2, our baseline non-proxy model. Further, the path-length mixing term improved the skill of the model in the subducted region from 32% to 50% of the volume variance. This proxy was included in all subsequent models, making Model 4 our baseline proxy model.

Although anomalous MLD is an important contributor to subduction (Trossman et al., 2009), its inclusion in the transfer term in Model 5 degraded the skill relative to Model 4. Two possible explanations are that the transfer of EDW between regions is not equivalent to subduction or that the MLD difference is redundant information. If the MLD difference primarily reflects MLD anomalies in the formation region, those MLD anomalies (essentially EDW thickness anomalies) may be highly correlated with the formation region volume, which has already been incorporated into the transfer term (9); including the MLD proxy may make the transfer doubly dependent on the EDW volume.

Ekman pumping may affect the subduction rate of EDW; however, in our simple model, subduction is implicit in the transfer between the two boxes; in any year the EDW may have been subducted either before or after the transfer, as the box regions are fixed in time. Thus we could not test this contribution from Ekman effects.

The southward velocity in the region should affect the volumes in both regions and the model was clearly sensitive to its addition (Table 2, Models 6–8). The addition of the velocity in the transfer term (Models 6 and 8) slightly (but significantly, see Appendix

improved the skill in the formation region from 58% for Model 4 to 64% for Models 6 and 8. However, there is an inconsistency in including velocity in the transfer term, but not in the loss term of the subducted region (Model 6) that caused a large drop in skill in the subducted region. Including velocity in the loss term (Models 7 and 8) improved the fit in the subducted region relative to Model 4. Note that the loss term in the subducted region does not affect the formation region volume in the model. Although Models 7 and 8 have similar skills in the two regions, Model 7 more clearly reproduces subducted region anomalies.

Improvements in the models are illustrated by comparing volumes from Model 2 (without proxies) and Model 7 with observed volumes (Fig. 14). The model with mixing and advection proxies (Model 7) reproduces much of the anomalous volumes in both regions on decadal time scales; the path-length mixing proxy reproduces particularly well the positive anomaly in the formation region in 1996–1997, which in turn creates a volume anomaly in the subducted region. Model 7, while clearly capturing more variability than Model 2, underestimates the large decrease in EDW volume in 2003–2005; this period has the smallest EDW volumes in the period examined (Fig. 2), as well as the least distinct histogram modes (Fig. 5). For these years the amount of constrained EDW is much less than half of the unconstrained EDW (not shown), the typical ratio over the study period. This typical ratio is reflected in the constant  $\alpha_0$ , the fraction of newly formed 17–19 °C water that is transferred to the subducted region as EDW.

## 6. Conclusions

The goal of this study was to characterize the processes that contribute most strongly to interannual-to-decadal variations of EDW and thereby to provide guidance for evaluating climate models. The model examined here has very simple physics, consistent with the observations available over 1–2 decades. Formation of EDW by heat fluxes was included explicitly; several

other processes were examined using proxies. The contributions of the various processes were examined by comparison with observed volumes.

The study produced some robust conclusions: (1) anomalies of formation by surface heat fluxes over the 17–19 °C outcrop are clearly reflected in EDW volume anomalies; (2) of the newly formed 17–19 °C water about 35% is transferred to the subducted region as EDW; (3) other losses in the formation region are well parameterized by the meandering of the nearby GS (using the path length); and (4) transfer and losses from the subducted region can be parameterized reasonably well by the geostrophic surface flow. Formation anomalies resulting from Ekman advection, excluding the effects of changes in outcrop area that are implicit in the heat flux formation, make a small, but significant contribution to modeled volumes. MLD anomalies do not contribute to model skill.

Our modeling study quantified the contributions of heat flux forcing, mixing and advection (subduction) anomalies to anomalies of EDW volume. Previous studies of the KE and GS regions have been divided on the importance of each process in accounting for STMW volume or thickness anomalies: Qiu and Chen (2006) emphasized the importance of mixing, as parameterized by KE path length variations in the North Pacific, over heat flux anomalies and Dong et al. (2007), whose study region overlapped extensively with our subducted region, emphasized the importance of advection over heat flux anomalies. More recent studies in the North Atlantic (Forget et al., 2011; Maze and Marshall, 2013) emphasized the importance of heat fluxes in the seasonal cycle of EDW; however, these studies did not address the source of interannual variations. In addition to evaluating the contribution of several processes to EDW anomalies on the interannual-to-decadal scale, we demonstrated that seasonal anomalies from the combined OAF flux/ISCCP fluxes are consistent with observed volume estimates, even with the stratification constraint. Our anomaly model was insensitive to the mean volume budget as all terms scaled with the mean formation rate.

More detailed observations are necessary to distinguish between different types of losses, to evaluate the contributions of various processes to outcrop area, to evaluate flux biases and their impact on estimates, and to determine the evolution of EDW beyond a simple change in location. These studies are being conducted using observations from the CLIMODE field program in the North Atlantic and from KESS in the North Pacific in conjunction with ocean circulation models. Several such detailed analyses are included in this issue.

## Acknowledgments

Our work benefited from many conversations and the sharing of information with other CLIMODE investigators, in particular, Terry Joyce, Young-Oh Kwon and Leif Thomas. Suggestions from three anonymous reviewers greatly improved the text. Data sources are listed in Table 1. K.A.K. was supported by the National Science Foundation through grant 0960648 (CLIMODE analysis) and by the National Aeronautics and Space Administration through grant NN08AR30G (Ocean Surface Topography Science Team). S.D. was supported by the National Science Foundation through grant 0958548 (CLIMODE analysis) and NOAA Atlantic Oceanographic and Meteorological Laboratory.

## Appendix A. Estimates of statistical significance

The likely relationship between several variables and the relative importance of several physical processes in accounting for changes in EDW volume was based on simple statistics: time-

lagged and unlagged correlations and the fraction of variance (skill) of a model. For each statistic a measure of the significance is needed.

### A.1. Correlations

We compared correlations  $\rho$  with an estimate of the threshold correlation for 95% significance. This threshold depends on the degrees of freedom  $N$ , which is derived from the time-lagged autocorrelation function  $R(t)$  of each of the two time series used for the correlation. The integral time scale  $\tau$  (e.g., Taylor, 1921) is estimated as the integral of  $R(t)$  out to the first zero-crossing  $t_0$  for each time series, as in Stammer and Böning (1992)

$$\tau = \int_0^{t_0} R(t) dt$$

The length of the time series is then divided by the average of the two estimates of  $\tau$  to obtain  $N$ . The integral time scale  $\tau$  gives a larger, but more robust, estimate of  $N$  than the commonly used  $t_0$ , owing to the sensitivity of the integral to the shape of the autocorrelation function. For this estimate of  $N$  to be sensible, the two time series must have comparable values of  $\tau$ , that is, one time series cannot have considerably more energy at higher frequencies than the other. Here possible large discrepancies in estimates of  $\tau$  are remedied by lowpass filtering one of the series. Further,  $\tau$  will be skewed by a large periodic signal; therefore, the annual and semi-annual harmonics of every time series are removed before computing  $N$  and the correlations.

Significance levels for correlations are found by transforming the correlation  $\rho$  to an approximately Normal variable  $w$

$$w = \frac{1}{2} \ln \left( \frac{1+\rho}{1-\rho} \right)$$

A correlation is significant at the  $\alpha$  level if  $w$  satisfies  $|\sqrt{N-3}w| \leq z_{\alpha/2}$ , where  $N$  is the number of degrees of freedom of the time series (Bendat and Piersol, 2000). A threshold significance level  $\rho_c$  is found by solving

$$\ln \left( \frac{1+\rho_c}{1-\rho_c} \right) = \frac{2z_{\alpha/2}}{\sqrt{N-3}}$$

to obtain  $\rho_c = (e^b - 1)/(e^b + 1)$ , where  $b = 2z_{\alpha/2}/\sqrt{N-3}$ .

### A.2. Lagged correlations

Evaluating the significance of time-lagged correlations was tested using a Monte Carlo simulation. The significance test for a time-lagged correlation is the same as that for the unlagged correlation above; however, determining whether an increase in the correlation  $\Delta\rho$  with a lag is significant requires an additional test. Suppose two time series (e.g., EDW volume in two regions) are significantly correlated when one series leads the other by a small  $\Delta t$ , but are only slightly less correlated at zero lag, owing to relatively long times scales in the anomalies. The null hypothesis is that the increase in the lagged correlation over the unlagged correlation arises from random components (noise) in the two time series, which is sufficient to overcome an expected decrease in correlation with  $\Delta t$ . The Monte Carlo test consisted of generating  $M$  pairs of time series that differed only by the added noise and comparing the actual difference in correlation with a 95% significance threshold estimated from the  $M$  simulations.

The Monte Carlo procedure requires some estimates of the noise and then simulations that can be repeated to estimate thresholds (significance levels). First, each of the two series was normalized by removing its mean and periodic signals (here, the annual and semi-annual harmonics) and dividing by its standard deviation. Large discrepancies in the integral time scale  $\tau$  were

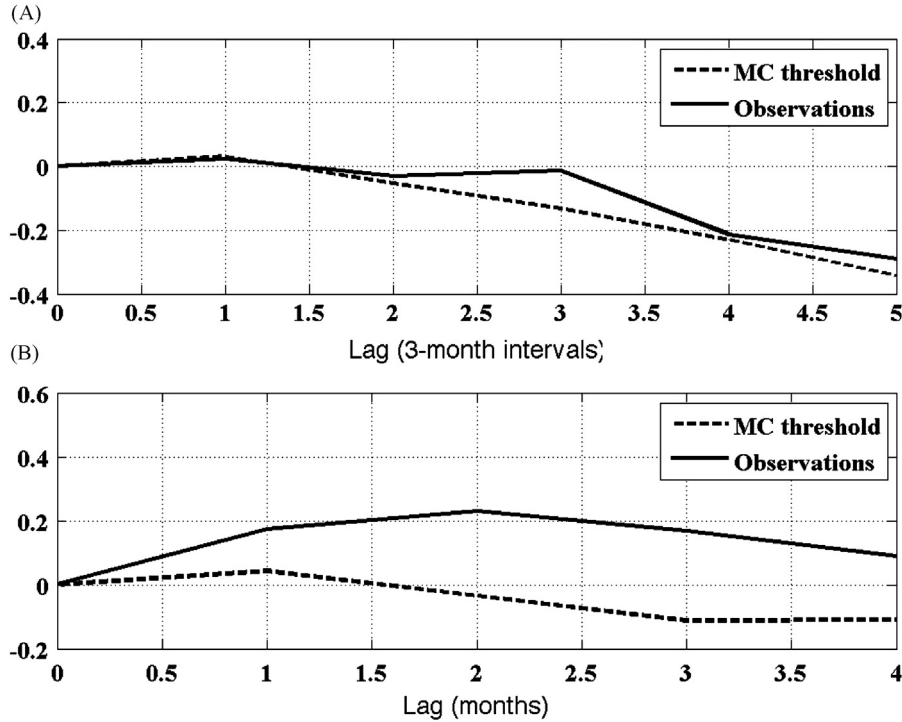


**Fig. 15.** Lagged correlation tests using Monte Carlo method. Actual (solid line) and threshold correlation difference (dashed line) for 95% significance level for (A) EDW in the formation region leads EDW in the subducted region and (B) SSH leads surface heat loss. (A) EDW volume lagged correlation test and (B) SSH vs.  $Q_{net}$  lagged correlation test.

resolved by lowpass filtering the series with the smaller value of  $\tau$  using the larger value of  $\tau$  for the half-power point of the filter. The filtered normalized time series were used for the lagged correlations.

The null hypothesis is that the correlated time series are actually two realizations of the same underlying common times series  $f$ , but with noise added:  $F_1(t) = f(t) + \epsilon_1(t)$  and  $F_2(t) = f(t) + \epsilon_2(t)$ . The mean-squared-difference of the series gives an estimate of the size of the errors  $\epsilon$

$$\langle [F_1(t) - F_2(t)]^2 \rangle = \langle \epsilon_1(t)^2 \rangle + \langle \epsilon_2(t)^2 \rangle = 2\epsilon^2$$

where  $\langle \cdot \rangle$  is the expected value, here the time average, and the errors in the two (normalized) time series are assumed to be comparable in size. An underlying time series  $f$  was generated by averaging the two normalized series and then smoothing it to remove the residual errors; the half power of this filter was the average value of  $\tau$  for the adjusted time series.

The Monte Carlo simulations consisted of generating pairs of new time series  $f_1(t) = f(t) + n_1(t)$  and  $f_2(t) = f(t) + n_2(t)$ , where  $n_i$  was normally distributed random noise with standard deviation  $\epsilon$ . (In the case of the EDW volumes, for which the 3-month average volumes were interpolated to monthly values, the noise was generated at 3-month intervals and then interpolated to monthly values to simulate the observations.) For each pair lagged correlations were performed between  $f_1(t)$  and  $f_2(t)$ , and the difference between the lagged and unlagged correlation was computed (for each lag); this process was repeated  $M=5000$  times. The  $M$  sets of correlation differences  $\Delta\rho(\Delta t)$  (lagged minus unlagged) were sorted in decreasing order, with the 0.05  $M$  largest correlation representing the 95% threshold for the difference in correlations. For small values of  $n_i(t)$  the threshold difference will decrease with lag, while for large values the threshold difference will increase slightly. For one series to significantly lag the other, the increase in correlation at lag  $\Delta t$  must exceed the threshold correlation difference at that lag.

For the EDW volume time series, the highest correlation occurred when EDW in the subducted region lags EDW in the formation region by 3 months (one time step for the quarterly averaged data). The lagged correlation was 0.68 [0.36], while the unlagged correlation was also significant at 0.66; however, the correlation difference  $\Delta\rho(\Delta t)$  for a lag of 3 months is just below the 95% threshold, whereas  $\Delta\rho(\Delta t)$  for lags of 6 and 9 months are significant (Fig. 15a).

For net surface heat loss,  $-Q_{net}$ , and SSH (as a proxy for heat content) in the formation region, the highest correlation occurred when SSH leads (negative) flux by 2 months. The lagged correlation was 0.32 [0.22], while the unlagged correlation (0.10) was not significant. The correlation difference  $\Delta\rho(\Delta t)$  exceeds the 95% threshold at lags of 1 month or more (Fig. 15b).

### A.3. Multiple parameters

In the models incorporating multiple processes, an estimate of the significance of adding another variable is needed to determine whether one model is better than another. The relevant statistic is the fraction of signal variance  $\sigma^2$  (here the variance of observed EDW volumes) that is described by the model, also called the “skill”  $S$  of the model

$$S = 1 - \frac{\langle \epsilon^2 \rangle}{\sigma^2}$$

where  $\epsilon$  is the model error and  $\langle \cdot \rangle$  represents the expected value (approximated as the time-average).

In linear regressions adding a variable will always increase  $S$  over one using fewer variables because the coefficients for the variable are optimized to minimize the fit to the observations. The models examined here are similar to a linear regression, in that some coefficients are empirical; however, all the proxies are normalized and constrained to be positive because a negative value would be inconsistent with the assumed dynamical relationship. For a multivariate linear regression a simple rule-of-thumb

(based on a  $F$ -test) is that an additional variable should decrease the residual squared error by  $1/N$  (Davis, 1977). If the fractional squared error from the initial model (for example, Model 2) is given by  $\epsilon_0^2/\sigma^2$ , then to be significant the addition of another variable should increase the skill by at least

$$\Delta S > \frac{\langle \epsilon_0^2 \rangle}{\sigma^2 N}$$

All the skill comparisons were based on the same time record (1993–2007), for which we estimate  $N=17$ . For example, the improvement of Model 4 over Model 2 is  $\Delta S=0.19$  (Table 2); the minimum value is  $(1-0.39)/17=0.04$ , which makes the model improvement clearly significant. The improvement of Model 8 over Model 5 in the subtropical region is  $\Delta S=0.03$  (Table 2), compared with the minimum value of  $(1-0.50)/17=0.03$ , which is not significant.

## References

- Bendat, J., Piersol, A., 2000. Random Data: Analysis Measurement Procedures. Wiley-Interscience, New York 594 pp.
- Davis, R.E., 1977. Techniques for statistical analysis and prediction of geophysical fluid systems. *Geophys. Astrophys. Fluid Dyn.* 8, 245–277.
- Davis, X.J., Straneo, F., Kwon, Y.-O., Kelly, K.A., Toole, J.M., 2013. Evolution and formation of North Atlantic Eighteen Degree Water in the Sargasso Sea from moored data. *Deep-Sea Res.* II 91, 11–24.
- Dong, S., Hautala, S., Kelly, K.A., 2007. Interannual variations in upper ocean heat content and heat transport convergence in the western North Atlantic. *J. Phys. Oceanogr.* 37, 2682–2697.
- Dougllass, E.M., Kwon, Y.-O., Jayne, S.R., 2013. A comparison of subtropical mode waters in a climatologically-forced model. *Deep-Sea Res.* II 91, 139–151.
- Ducet, N., Traon, P.-Y.L., Reverdin, G., 2000. Global high-resolution mapping of ocean circulation from TOPEX/Poseidon and ERS-1 and -2. *J. Geophys. Res.* 105, 19477–19498.
- Forget, G., Maze, G., Buckley, M., Marshall, J., 2011. Estimated seasonal cycle of North Atlantic Eighteen Degree Water volume. *J. Phys. Oceanogr.* 41, 269–286.
- Huang, R.X., Qiu, B., 1994. Three-dimensional structure of the wind-driven circulation in the subtropical North Pacific. *J. Phys. Oceanogr.* 24, 1608–1622.
- Hurrell, J.W., Kushnir, Y., Ottersen, G., Visbeck, M., 2003. An overview of the North Atlantic Oscillation. In: Hurrell, J.W., Kushnir, Y., Ottersen, G., Visbeck, M. (Eds.), *The North Atlantic Oscillation*, American Geophysical Union Geophysical Monograph, vol. 134, pp. 1–35.
- Joyce, T., Thomas, L.N., Dewar, W.K., Girton, J.B., 2013. Eighteen Degree Water formation within the Gulf Stream: a new paradigm arising from CLIMODE. *Deep-Sea Res.* II 91, 1–10.
- Joyce, T.M., Deser, C., Spall, M.A., 2000. The relation between decadal variability of Subtropical Mode Water and the North Atlantic Oscillation. *J. Clim.* 13, 2550–2569.
- Kelly, K.A., Small, R.J., Samelson, R., Qiu, B., Joyce, T.M., Cronin, M., Kwon, Y.-O., 2010. Western boundary currents and frontal air–sea interaction: gulf stream and Kuroshio extension. *J. Clim.* 23, 5644–5667.
- Kwon, Y.-O., 2003. Observation of General Circulation and Water Mass Variability in the North Atlantic Subtropical Mode Water Region. Ph.D. thesis, University of Washington, 161 pp.
- Kwon, Y.-O., Riser, S.C., 2004. North Atlantic subtropical mode water: a history of ocean–atmosphere interaction 1961–2000. *Geophys. Res. Lett.* 31, <http://dx.doi.org/10.1029/2004GL021116>.
- Levitus, S.J., Antonov, I., Boyer, T.P., Locarnini, R.A., Garcia, H.E., Mishonov, A.V., 2009. Global ocean heat content 1955–2008 in light of recently revealed instrumentation problems. *Geophys. Res. Lett.* 36, L07608, <http://dx.doi.org/10.1029/2008GL037155>.
- Maze, G., Forget, G., Buckley, M., Marshall, J., Cerovecki, I., 2009. Using transformation and formation maps to study the role of air–sea fluxes in North Atlantic Eighteen Degree Water formation. *J. Phys. Oceanogr.* 39, 1818–1835.
- Maze, G., Marshall, J., 2013. Comparison of North Atlantic and North Pacific subtropical mode water formation processes. *Deep-Sea Res.* II 91, 128–138.
- Monterey, G., Levitus, S., 1997. Seasonal Variability of Mixed Layer Depth for the World Ocean. NOAA Atlas NESDIS 14, National Oceanic and Atmospheric Administration, Silver Spring, MD, 100 pp.
- Olsina, O., Wienders, N., Dewar, W.K., 2013. The climatology and variability of Eighteen Degree Water potential vorticity forcing. *Deep-Sea Res.* II 91, 84–95.
- Qiu, B., Chen, S., 2006. Decadal variability in the formation of the North Pacific subtropical mode Water: oceanic versus atmospheric control. *J. Phys. Oceanogr.* 36, 1365–1380.
- Qiu, B., Chen, S., Hacker, P., 2007. Effect of mesoscale eddies on subtropical mode Water variability from the Kuroshio Extension system study (KESS). *J. Phys. Oceanogr.* 37, 982–1000.
- Qiu, B., Huang, R.X., 1995. Ventilation of the North Atlantic and the North Pacific: subduction versus obduction. *J. Phys. Oceanogr.* 25, 2374–2390.
- Rainville, L., Jayne, S.R., McClean, J.L., Maltrud, M.E., 2007. Formation of Subtropical Mode Water in a high-resolution ocean simulation of the Kuroshio Extension region. *Ocean Modell.* 17, 338–356.
- Rajamony, J., Herbert, D., Rossby, T., 2001. The cross-stream potential vorticity front and its role in meander-induced exchange in the Gulf Stream. *J. Phys. Oceanogr.* 31, 3551–3568.
- Reynolds, R.W., Smith, T.M., Liu, C., Chelton, D.B., Casey, K.S., Schlax, M.G., 2007. Daily high-resolution-blended analyses for sea surface temperature. *J. Clim.* 20, 5473–5496.
- Rio, M.-H., Hernandez, F., 2004. A mean dynamic topography computed over the world ocean from altimetry, in situ measurements, and a geoid model. *J. Geophys. Res.* 109, C12032, <http://dx.doi.org/10.1029/2003JC00222>.
- Schiffer, R.A., Rossow, W.B., 1983. The international satellite cloud climatology project (ISCCP): the first project of the World Climate Research Programme. *Bull. Am. Meteor. Soc.* 64, 779–784.
- Siedler, G., Kuhl, A., Zenk, W., 1987. The Madeira mode Water. *J. Phys. Oceanogr.* 17, 1561–1570.
- Speer, K., Tziperman, E., 1992. Rates of water mass formation in the North Atlantic Ocean. *J. Phys. Oceanogr.* 22, 93–104.
- Stammer, D., Böning, C.W., 1992. Mesoscale variability in the Atlantic Ocean from Geosat altimetry and WOCE high-resolution numerical modeling. *J. Phys. Oceanogr.* 22, 732–752.
- Suga, T., Aoki, Y., Saito, H., Hanawa, K., 2008. Ventilation of the North Pacific subtropical pycnocline and mode water formation. *Prog. Oceanogr.* 77, 285–297.
- Talley, L.D., Raymer, M.E., 1982. Eighteen degree water variability. *J. Mar. Res.* 40 (Suppl.), 757–775.
- Taylor, G.I., 1921. Diffusion by continuous moments. *Proc. London Math. Soc.* 20, 196–212.
- The CLIMODE Group, 2009. Observing the cycle of convection and restratification over the Gulf Stream and the subtropical gyre of the North Atlantic Ocean: preliminary results from the CLIMODE field campaign. *Bull. Am. Meteor. Soc.* 90, 1337–1350.
- Thomas, L.N., 2005. Destruction of potential vorticity by winds. *J. Phys. Oceanogr.* 35, 2466–2547.
- Trossman, D., Thompson, L., Kelly, K., Kwon, Y.-O., 2009. Estimates of North Atlantic ventilation and mode Water formation for winters 2002–2006. *J. Phys. Oceanogr.* 39, <http://dx.doi.org/10.1175/2009JP03930.1>.
- Walsh, G., 1982. On the relation between sea-surface heat flow and thermal circulation in the ocean. *Tellus* 34, 187–195.
- Warren, B.A., 1972. Insensitivity of subtropical mode water characteristics to meteorological fluctuations. *Deep-Sea Res.* II 19, 1–19.
- Weller, R.A., Bigorre, S., Edson, J., 2013. In-situ surface meteorology and air–sea fluxes in and near the Gulf Stream at 38°N, 65°W. *Deep-Sea Res.* 91, 71–83.
- Worthington, L.V., 1976. On the North Atlantic Circulation, vol. 6. Johns Hopkins Oceanographic Studies, 110 pp.
- Yu, L., Weller, R.A., 2007. Objectively analyzed air–sea heat fluxes for the global ice-free oceans (1981–2005). *Bull. Am. Meteor. Soc.* 88, 527–539.